Cite this: DOI: 10.1039/c0xx00000x

www.rsc.org/xxxxxx

ARTICLE TYPE

Unique photo-activation mechanism by "*in situ doping*" for photo-assisted selective NO reduction with ammonia over TiO_2 and photooxidation of alcohols over Nb_2O_5

Tetsuya Shishido,*[a] Kentaro Teramura[a] and Tsunehiro Tanaka[a]

Received (in XXX, XXX) Xth XXXXXXXXX 200X, Accepted Xth XXXXXXXXX 200X
DOI: 10.1039/b000000x

This paper reviews the recent development of the photocatalytic emission control reaction and photooxidation with molecular oxygen, specifically focusing on efforts based on the revealing the reaction mechanism by the authors' group. TiO_2 acts as an effective catalyst for the photo-assisted selective catalytic reduction of NO with NH_3 in the presence of O_2 (photo-SCR). Photooxidation of alcohols to carbonyl compounds proceeds selectively over Nb_2O_5 without organic solvents. Usually, both TiO_2 and Nb_2O_5 work only in the ultraviolet (UV) region because of the limit of their bandgap energies. However, both photo-SCR over TiO_2 and photooxidation of alcohols over Nb_2O_5 proceed even under visible light irradiation up to ca. 450 nm. This indicates that these two reactions take place by the different photo-activation mechanism from the classical electron transfer mechanism in semiconductor photocatalysis, that is, the formation of an excited electron in the conduction band and the positive hole in the valence band. A mechanistic study using UV-Vis, ESR, FT/IR, kinetic study, and DFT calculations revealed the reaction mechanisms of photo-SCR and photooxidation of alcohols, and that the surface complex consisting of adsorbed molecule and catalyst plays an important role in the photo-activation step. The surface complex is converted to the photo-activated species even under visible light irradiation, because the direct electron transition from a donor level derived from adsorbed molecule to the conduction band of photocatalyst takes place and photo-generated hole is trapped on adsorbed molecule to form the photo-activated radical species. The effective wavelength is shifted to a longer wavelength by the formation of donor level derived from adsorbed molecule during a chemical reaction (called here "*in situ doping*"). This unique photo-activation mechanism by "*in situ doping*" gives us attractive ways for the removing the limit of bandgap energy, and the utilization of visible light.

1. Introduction

As shown in Scheme 1, photocatalytic reactions on a semiconductor powder involves several steps. Photocatalysis is generally explained in terms of band theory (the classical electron transfer mechanism) accompanied by the interaction of reactants with the photo-generated electrons and holes, and is potentially available to make the catalytic reactions proceeding at low temperature. The band structure of the photocatalysts determines the utilizable light energy, oxidizability, and reducing ability. It has been considered that suppressing recombination between photo-generated electrons and holes in a photocatalyst is important to achieving the reaction, since the lifetime of the charge separation contributes to the photocatalytic activity. Therefore, a number of studies are related to the control of band structure and charge separation. On the other hand, little information about the adsorbed species and the intermediates in photocatalytic reactions is available. Photocatalytic reactions take place on the surface of the photocatalysts as well as the ordinary

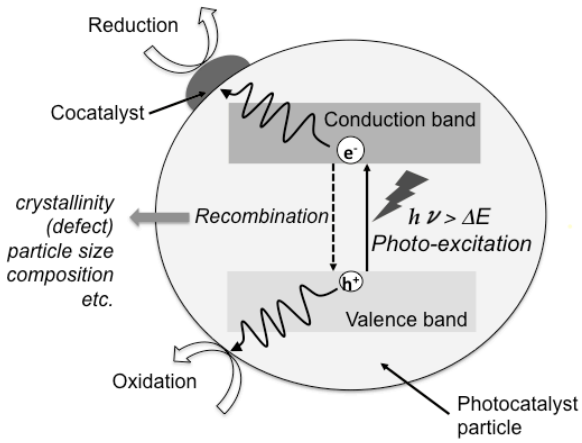

Scheme 1 Model of reaction, charge separation, and recombination over photocatalyst

catalysts. The difference between the photocatalysts and the ordinary catalysts is just the driving force to activate the adsorbed

reactants; the photocatalysts use the photo-energy and the ordinary catalysts use the thermal energy. Therefore, the kinetic interpretation and the knowledge of surface structure, surface property, and surface species during the photo-reaction are required to understand the photocatalysis; generally a catalytic reaction consists of several elementary steps and one or two of the elementary steps involves absorption of light in the case of a photocatalytic reaction. Hence, there is the same thermodynamic restriction in the photocatalysis with the ordinary catalysis. Evidently, it is necessary to consider the photo-activation mechanism in detail. The clarification of the reaction mechanism provides the beneficial information on the further improvement of the photocatalysis and a new insight of photocatalytic chemistry.

This article summarizes our recent work on the photo-activation mechanisms of NH_3 over TiO_2 in photo-SCR, and alcohols over Nb_2O_5 in the photooxidation with molecular oxygen. We show a detailed investigation of reaction mechanisms of photo-SCR over TiO_2 and selective photooxidation of alcohols over Nb_2O_5 using *in situ* characterization, kinetic study and DFT calculations. A redshift of effective wavelength due to the direct electron transition from the donor level derived from adsorbed molecule to the conduction band ("*in situ doping*") is demonstrated.

2. Photo-assisted selective reduction of NO with NH_3 over TiO_2 based catalysts

2.1 Low-temperature NH_3-SCR systems

The growth of the global economy involved the environmental problems such as solid, air and water pollutions. These pollutions cause serious damage to human and nature. In order to solve these problems, many efforts are under going for the development of the environmental technology.

NO*x* is one of the environmental pollutants and causes acid rain and photochemical smog. Therefore, it is desirable to remove NO*x* (de-NO*x*) in the stationary emission source and the mobile emission source. In the stationary emission source such as a thermal power station, an industrial boiler and a waste incinerator, NO*x* is conventionally removed from the exhaust gas by the selective catalytic reduction system with NH_3 as a reductant (NH_3-SCR) in the presence of the excess O_2 over V_2O_5-WO_3 (or V_2O_5-MoO_3)/TiO_2 catalyst.[1-4] This technology was invented by three Japanese corporations (Hitachi Ltd., Babcock-Hitachi K. K., Mitsubishi Petrochemical Corp.).[5] The reaction stoichiometry in the typical NH_3-SCR is shown as follows;

$$4NO + 4NH_3 + O_2 \rightarrow 4N_2 + 6H_2O \quad (1)$$

N_2 is formed by the reaction of NO with NH_3.[6-11] N_2O is a by-product. This system shows high NO conversion (99%), high N_2 selectivity (> 90%) and resistance for H_2O and SO*x*, although the catalyst requires high operating temperature (573−673 K).[12] Since the exhaust gas contains various pollutants and materials such as SO*x*, halogen compounds, particulate matter (PM) and fly ash in addition to NO*x*, the NH_3-SCR system is used together with de-SO*x*, de-halogen and dust collection systems. Thus, the NH_3-SCR system is often located downstream of the de-SO*x*, de-halogen and dust collection systems in order to inhibit deactivation of V_2O_5-WO_3 (or V_2O_5-MoO_3)/TiO_2 catalyst. In this case, the inlet temperature of the exhaust gas in the NH_3-SCR system falls below 453 K. Consequently, it is necessary to re-heat the catalysis bed and the gas up to the operating temperature of the catalyst. Therefore, it is desired to develop a new de-NO*x* system working at low temperature (< 453 K). Since the 1990s, the low-temperature NH_3-SCR has been investigated to develop the new NH_3-SCR system capable of operating under 453 K. The following is requested feature of the low-temperature NH_3-SCR system: (1) NO*x* conversion must be high (more than 90%), (2) N_2 selectivity must be high (more than 90%), (3) catalysts must have high durability to H_2O, and (4) NH_3-SCR system must be operated in the presence of an excess O_2. Since H_2O vapor gets mixed in with the exhaust gas in the de-SO*x* and the de-halogen processes, the catalysts must have high durability to H_2O. The low-temperature NH_3 SCR systems reported are listed in Table 1.[13-19] The first report of the NH_3-SCR is MnO_2-Al_2O_3 catalyst reported by Singoredjo et al.[14] MnO_2-Al_2O_3 catalyst had poor durability to H_2O and the activity decreased with the course of the reaction time.

Table 1 Low-temperature SCR reaction systems

Catalyst	Reaction gas composition				Reaction condition		Activity		Ref.
	NO (ppm)	NH_3 (ppm)	O_2 (ppm)	H_2O (%)	T (K)	SV (h^{-1})	X_{NO} (%)	S_{N2} (%)	
MnO_2-Al_2O_3	550	550	2	0	435	31,000	98	92	11
MnO_2-carbonized silica-alumina	800	800	3	0	413	12,000	94	91	13
MnO_2-NaY	1000	1000	10	7	443	48,000	88	93	
MnO_2-TiO_2	2000	2000	2	0	393	8,000	100	100	17
MnO_2-TiO_2	400	400	2	11	448	50,000	98	97	
Fe-Mn oxide	1000	1000	2	0	393	15,000	100	100	19
Fe-Mn oxide	1000	1000	2	2.5	413	15,000	98	100	
MnO_2-CeO_2	1000	1000	2	0	393	42,000	99	100	16
MnO_2-CeO_2	1000	1000	2	19	393	42,000	95	100	
V_2O_5-sulphated carbon	500	600	3	0	453	34,000	92	100	15

[a] T: Reaction temperature, SV: Space velocity, X_{NO}: NO conversion, S_{N2}: N_2 selectivity

Cite this: DOI: 10.1039/c0xx00000x

www.rsc.org/xxxxxx

ARTICLE TYPE

Subsequently, several Mn-containing catalysts, which show the high activity with the durability to H_2O at a low-temperature, are reported.[13-15, 17, 18] Among the Mn-containing catalysts reported, MnO_2-CeO_2 shows the highest activity (95% NO conversion and 100% N_2 selectivity in the presence of 19% H_2O).[17]

2.2 Photo-SCR with NH_3 over TiO_2 Photocatalysts

Over the past decades, the most attentions of the photocatalysis have been gathered to the water photolysis and the removal of harmful compounds over photocatalysts responding to visible light. In contrast, although photocatalysts have the advantage that the re-heating of catalyst bed is unnecessary because of their possibility of application at low temperatures, the reports of the NH_3-SCR reaction over photocatalysts (photo-SCR) were limited. Cant et al. reported that NO reduction by NH_3 to form N_2 proceeds over TiO_2 under photo-irradiation.[20] The reaction was carried out in a closed system and the activity was very low. On the contrary, we found that TiO_2 and metal oxide promoted TiO_2 are effective for the photo-SCR with NH_3 in the presence of O_2 proceeds at room temperature.[21-29]

Table 2 shows the catalytic activity and physicochemical property of photo-SCR with NH_3 over various TiO_2 photocatalysts (JRC-TIO-1-13 supplied from Catalysis Society of Japan). JRC-TIO-11, a mixture of rutile and anatase phases, exhibited the highest activity among all TiO_2 tested. JRC-TIO-8 and JRC-TIO-3 were the most active catalysts consisting of anatase or rutile single phases. There is poor correlation between the activity and crystal phase, crystallite size, and specific surface area. This indicates that these properties are not the important factors to determine the activity of photo-SCR.

Table 2 Activities of photo-SCR reaction with NH_3 over various TiO_2 photocatalysts

Catalysts	*Sa* (m^2/g)	Phase	D_c (Å)	NO conv. (%)	N_2 sel. (%)
JRC-TIO-1	71.1	A	187	36	100
JRC-TIO-2	15.6	A	535	14.5	100
JRC-TIO-3	45.6	R	219	53	100
JRC-TIO-4	47.8	R 29.4%	382	35.5	100
		A 70.6 %	259		
JRC-TIO-5	3 ~ 4	R 92.4 %	2200	31	100
		A 7.6 %	1000		
JRC-TIO-6	58.0	R	240	20	100
JRC-TIO-7	108	A	197	35	100
JRC-TIO-8	93.2	A	155	51.7	98.6
JRC-TIO-9	95.2	A	197	31	100
JRC-TIO-10	100	A	169	35.5	100
JRC-TIO-11	76.6	R 8.7 %	200	63	100
		A 91.3 %	153		
JRC-TIO-12	98.7	A	159	41	100
JRC-TIO-13	71.1	A	237	33	100

[a] A : anatase, R : rutile. Reaction condition; NO: 1000ppm, NH_3: 1000ppm, O_2: 2%, Ar balance, GHSV = 32000 h^{-1}

2.3 Mechanism of photo-SCR with NH_3 over TiO_2 photocatalysts

Figure 1 shows the EPR spectra of TiO_2. After evacuation at 673 K, the signals are derived from the Ti^{3+} species (Fig. 1 (a)).[30-33] There is little change in EPR signal by the exposure of NH_3 to TiO_2 in the dark. On the other hand, EPR signal changed drastically after photo-irradiation. New signals assignable to NH_2 radical[34-38] were detected together with signals assigned to Ti^{3+}. These new signals were quite stable even after more than 1 hour at 123 K without photo-irradiation. However, these signals immediately vanished by the exposure to NO in the dark whereas the intensity of signals due to Ti^{3+} species increased. This suggests that 1) the photo-generated electron is trapped on Ti^{4+} to form Ti^{3+} and positive hole is captured by adsorbed NH_3 species to convert to active NH_2 radical, and that 2) NO in the gas phase attacks the NH_2 radical on TiO_2 rapidly. As both NH_2 radical and NO are doublet state species, it follows that NH_2 radical reacts with NO easily without irradiation. Moreover, the formation of a NH_2NO intermediate was confirmed by FTIR spectroscopy after admittance of NO to TiO_2 adsorbing NH_3 under photo-irradiation (vide infra). As described above, the signals due to Ti^{3+} species increased in intensity after the introduction of NO. It seems that the electron transfer took place from the N atom of adsorbed NH_3 to the Ti atom of TiO_2 bulk. In other words, the photo-generated electron was trapped on Ti atom and the photo-generated hole was captured by the NH_2^- species derived from adsorbed NH_3. As a result, the NH_2^- species converted to the active NH_2 radical. On the other hand, the electron may move into inside of TiO_2 bulk as a stable free electron. Before the exposure to NO, recombination took place between a part of Ti^{3+} species and the NH_2 radical. On the other hand, after the exposure to NO, the electron could not recombine because of losing an opponent (NH_2 radical). The electron was localized and stabilized in inside of TiO_2, and the signals assigned to the Ti^{3+} species increased in intensity.

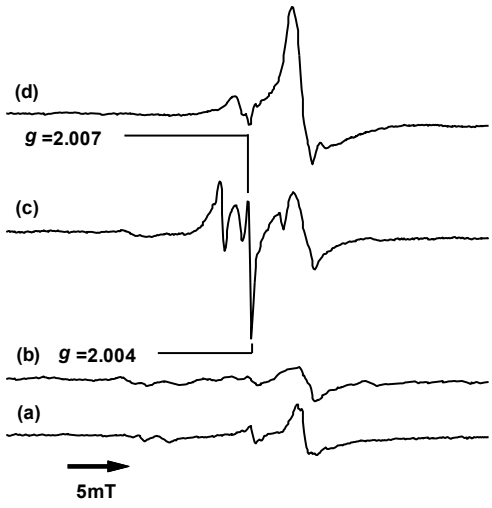

Fig. 1 EPR spectra of TiO_2 (a) after pretreatment, (b) after introduction of NH_3 in the dark, (c) under photo irradiation and (d) after introduction of NO in the dark.

Figure 2 shows the time course of N_2 evolution rate of photo-SCR. NO conversion and N_2 selectivity attained to 100 % and 96 % respectively in the conventional fixed bed flow system (GHSV = 8,000 h^{-1}). The N_2 evolution rate gradually increased at the initial stage and reached a steady rate at 1.5 h. However, when the reaction gas (a mixture of $NO/NH_3/O_2$) was passed in the dark for 0.5 h, and then photo-irradiation was started, the N_2 evolution rate immediately jumped to the level of the steady rate.[23, 25] This clearly indicates that the induction period shown in Fig. 2 is the time for saturation of the adsorption equilibrium of the reactant molecule. When NH_3 were passed for 1.5 h in the dark, then the gas was switched to a mixture of NO/O_2 and the photo-irradiation was started, N_2 was evolved. The N_2 evolution rate gradually decreased and the total amount of evolved N_2 was consistent with that of equilibrium adsorption of NH_3 on TiO_2. On the contrary, when a mixture of NO/O_2 were firstly passed and then switched to NH_3, neither N_2 nor N_2O was formed. These results suggest that NH_3 species adsorbed on Lewis acid site is excited by photo-irradiation and reacts with NO in the gas phase to produce N_2. Furthermore, this is supported by the fact that only $^{15}N^{14}N$ was evolved in the photo-SCR of ^{15}NO with $^{14}NH_3$ in the presence of O_2.[22]

The adsorbed species and intermediates of photo-SCR were identified by *in situ* FT/IR spectra (Fig. 3). After NH_3 adsorbed on TiO_2, the bands (1136, 1215, and 1599 cm^{-1}) due to adsorbed NH_3 species on Lewis acid site of TiO_2 appeared.[39-41] The bands at 1599 and 1215 cm^{-1} retained their intensity after evacuation (Fig. 3 (b)) and exposure to NO in the dark (Fig. 3 (c)). The bands due to adsorbed NH_3 decreased gradually in intensity with irradiation time. On the other hand, the band at 1624 cm^{-1}, which is assignable to the deformation vibration of H_2O[42], grew. Furthermore, new bands between 1400 and 1600 cm^{-1} were observed and then disappeared. These new bands are assigned to the nitrosamide species (NH_2NO) by comparing the FT/IR spectrum of TiO_2 exposed with ^{14}NO and NH_3 to that exposed with ^{15}NO and NH_3.[24]

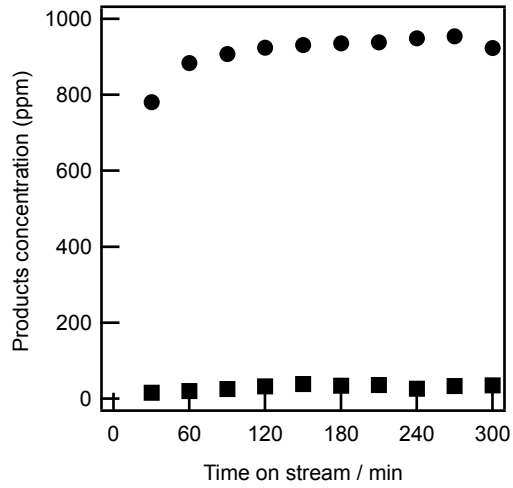

Fig. 2 Time course of N_2 (circle) and N_2O (triangle) in the photo-SCR with NH_3 over TiO_2 JRC-TIO-11, Reaction condition; GHSV = 8000 h^{-1}, NO: 1000ppm, NH_3: 1000ppm, O_2: 2%, Ar balance

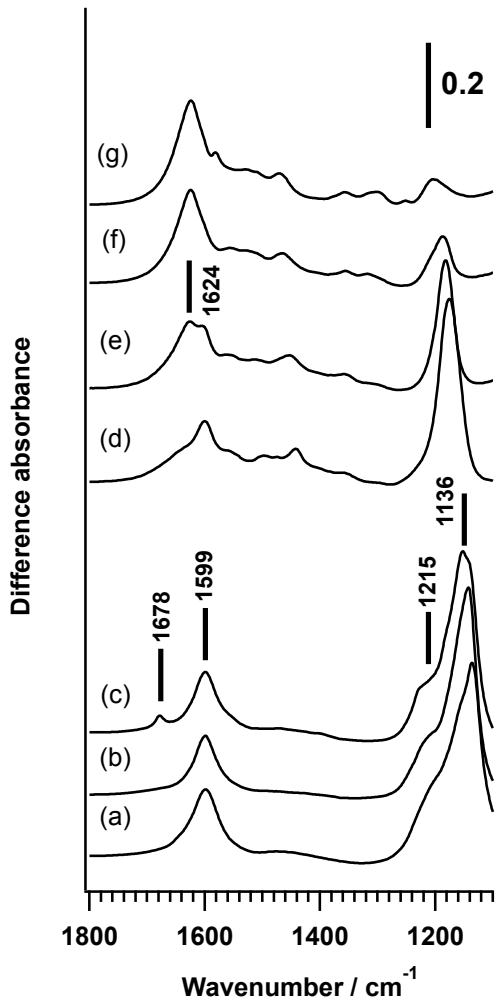

Fig. 3 FT-IR spectra of adsorbed species on TiO_2 in the photo-SCR with NH_3. (a) after introduction of NH_3, (b) after evacuation, (c) after introduction of NO in the dark, (d) under photo irradiation for 10 min, (e) for 30 min, (f) for 60 min, and (g) for 120 min.

These results indicate that the intermediate of photo-SCR is the nitrosamide species (NH_2NO) and the nitrosamide species is decomposed to N_2 and H_2O. Moreover, it was confirmed that the Ti^{3+} species of TiO_2 reduced by H_2 was re-oxidized to the Ti^{4+} species by exposure to O_2 easily even at room temperature using UV-Vis spectroscopy.[27] On the basis of these results, we proposed Eley-Rideal type mechanism as follows (Scheme 2) [24-29]; 1) the NH_3 adsorbs on Lewis acid site of TiO_2, 2) the adsorbed NH_3 species is excited by photo-irradiation, 3) the excited species (NH_2 radical) reacts with NO in the gas phase to form the nitrosamide species (NH_2NO), 4) the nitrosamide species is decomposed to N_2 and H_2O, and 5) Ti^{3+} site is re-oxidized by molecular oxygen.

According to the dependencies of the partial pressure of NO, NH_3, and O_2, the reaction rate (r) of photo-SCR is expressed as [Eq.(2)].

$$r = k\, P_{NH3}^{0.0}\, P_{NO}^{0.5}\, P_{O2}^{0.07} \qquad (2)$$

Here, the rate constant, the partial pressure of NH_3, NO, and O_2 are abbreviated to k, P_{NH3}, P_{NO}, and P_{O2}, respectively. This equation indicates that NH_3 adsorbs strongly on TiO_2 (Step 1) and that re-oxidation of Ti^{3+} to Ti^{4+} (Step 5) proceeds rapidly. By comparing the obtained rate equation [Eq. (2)] with the rate equation derived from the proposed reaction mechanism by steady-state approximation, we concluded that Step 4, the decomposition of the nitrosamide species, is the rate-determining step of photo-SCR.

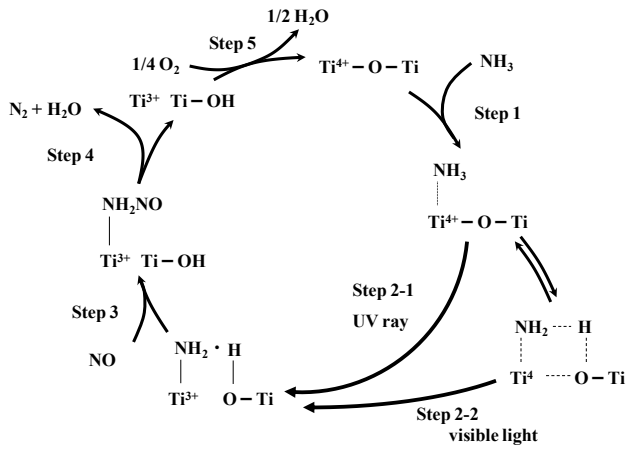

Scheme 2 Reaction mechanism of photo-SCR with NH_3 over TiO_2

2.4 Enhanced of activity by improving of lifetime of photo-activated species

An efficient charge separation promotes the chemical reactions competing with a recombination of the photo-generated electrons and holes. Einaga et al. reported that benzene as a model VOCs (volatile organic compounds) can be abated by total oxidation over TiO_2 photocatalyst effectively.[43-45] However, the specific activity of TiO_2 is absolutely low. They reported that 120 ppm of benzene cannot be removed over TiO_2, but 80 ppm of benzene is efficiently decomposed to CO_2 and CO in the presence of H_2O vapor. This would be caused by the insufficient lifetime of charge-separated state over TiO_2. It is widely thought that the photo-generated electrons and holes are consumed by

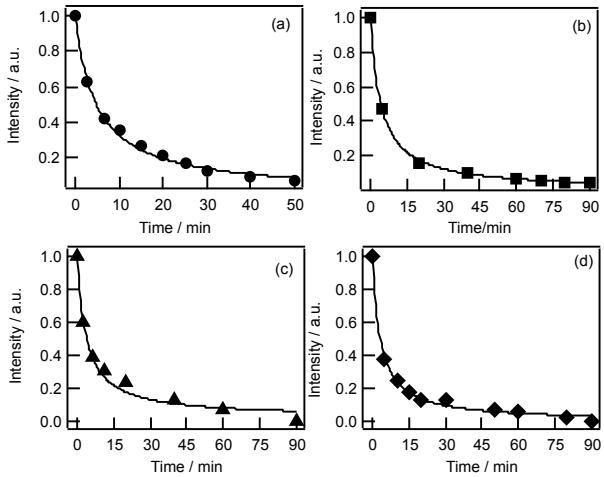

Fig. 4 Decay curve of NH_2 radical and the approximated curve (liners) at (a) 113 K, (b) 123 K, (c) 133 K and (d) 143 K.

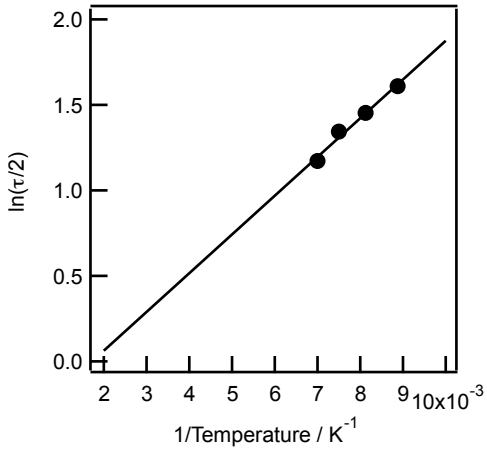

Fig. 5 Arrhenius plots of the half-lives of NH_2 radical at each temperature (dot) and the approximated line (liner).

recombination much more rapidly than by the photocatalytic reaction and the recombination is the main reason of too short lifetime of the charge-separated state and resulting in low activity of TiO_2. Indeed, the half-life of charge-separated state of TiO_2 was estimated to be below 100 psec.[46, 47] Up to now, the limit of the extended lifetime of charge-separated state is only several ten of nsec despite the careful effort. Therefore, in the case of photo-SCR over TiO_2, it seems that the half-life of NH_2 radicals, which are formed by capturing photo-generated positive holes, is below 100 psec and that the rate-determining step of photo-SCR is the reaction of NH_2 radical with NO to form the nitrosamide species (NH_2NO). However, as described above, the kinetic study indicated that the decomposition of the nitrosamide species (Step 4) is the rate-determining step of photo-SCR. This strongly suggests that the strongly adsorbed NH_3 on Lewis acid site of TiO_2 lengthened the lifetime of the charge-separated state by trapping hole and consequently the recombination of the photo-generated electrons and holes is inhibited. Figure 4 shows the decay curve of NH_2 radical signal recorded by EPR after irradiation stopped. All decay curves can be approximated to a hyperbolic curve, indicating that NH_2 radical is quenched by the secondary reaction between NH_2 radical and electron. The half-

life of NH_2 radical at reaction temperature of photo-SCR (323 K) is calculated to be 1.4 min by using Arrhenius equation (Fig. 5). Since this half-life of the NH_2 radical at 323 K is much longer than that of the charge-separated state of TiO_2 (< 100 psec), the concentration of NH_2 radical on the surface of TiO_2 increased and the activity of photo-SCR is enhanced. To best of our knowledge, the intermediate and active species having a longer lifetime such as the NH_2 radical has not been reported.

2.5 Mechanism of formation of NH_2 radical over TiO_2

Figure 6 shows the apparent quantum efficiency of the photo-SCR over TiO_2 as a function of the incident light (action spectrum) and a UV-Vis spectrum of TiO_2. The band gap of this TiO_2 is estimated to 3.28 eV (photo-excitation energy is 385 nm). The action spectrum is in good agreement with the UV-Vis spectrum of TiO_2 in the region of wavelength < 385 nm. Although TiO_2 is unable to absorb light at wavelengths > 385 nm, photo-SCR proceeded under irradiation up to ca. 450 nm. The feature of this action spectrum is similar to the UV-Vis spectrum of N-doped TiO_2.[48] In order to reveal whether a new energy level derived from adsorbed molecule is located between the HOMO and LUMO levels or not, density functional theory (DFT) calculations were employed. DFT calculations revealed that N 2*p* electron donor level is located between O 2*p* and Ti 3*d* when NH_2 species are formed on a TiO_2 surface by the dissociatively-adsorption of NH_3.[27]

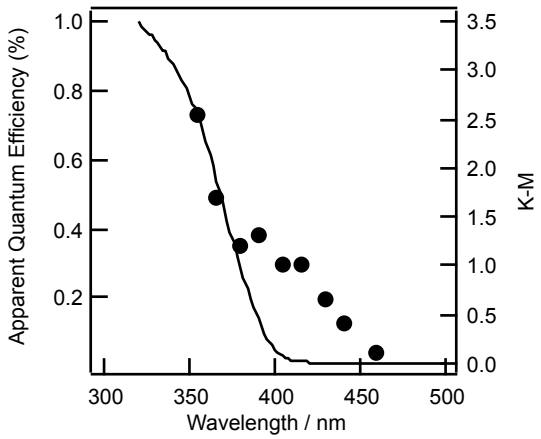

Fig. 6 Action spectrum of photo-SCR (dot) and UV-Vis spectrum of JRC-TIO-11 (liner); reaction condition of action spectrum: NH_3: 1000ppm, NO: 1000ppm, O_2: 2%, flow rate: 100 ml/min.

On the basis of these results, we conclude that the photo-activation of NH_3 adsorbed on TiO_2 to NH_2 radical occurs through two paths as shown in Fig. 7. One is the electron transition from the valence band consisting of O 2*p* orbitals to the conduction band consisting of Ti 3*d* orbitals of TiO_2 under UV irradiation. The other is the direct electron transfer from N 2*p* of adsorbed NH_3 to Ti 3*d*. This N 2*p* electron donor level formed between O 2*p* and Ti 3*d* enables the photo-SCR to proceed even under visible light irradiation (400-450 nm). It can be thought that the expansion of the effective wavelength of TiO_2 by adsorption of NH_3, called here, "*in situ doping*", is one of the factors for high activity of TiO_2 in the photo-SCR.

Many researchers reported that the "*pre-doped*" or "*pre-modified*" photocatalysts with metals or ions such as N-doped TiO_2 adsorb the visible light.[48-51] However, there has been no report that the effective wavelength of photo-reaction is shifted to a longer wavelength by the formation of donor level derived from adsorbed molecule on the catalyst during a chemical reaction ("*in situ doping*"). Moreover, "*in situ doping*" was found not only in photo-SCR with NH_3 over TiO_2 but also in the photooxidaiton of alcohols over Nb_2O_5. The detail of the photooxidaiton of alcohols over Nb_2O_5 is described in the next section.

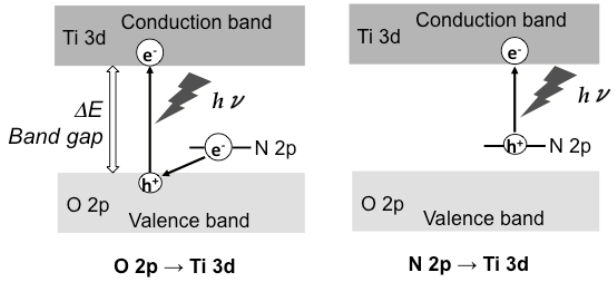

Fig. 7 Formation mechanism of NH_2 radical over TiO_2

3. Photooxidaiton of alcohols with molecular oxygen over Nb_2O_5 catalysts

3.1 Oxidation of alcohol with molecular oxygen

Catalytic alcohol oxidation to carbonyl compounds is one of the most important chemical transformations used in the industrial chemistry and in organic syntheses.[52-54] Non-catalytic methods with stoichiometric, toxic, corrosive and expensive oxidants such as ClO^-, dichromate, permanganate, and peroxy acids under stringent conditions of high pressure and/or temperature have been widely used for alcohol oxidations.[52-55] In addition, these reactions are often carried out with high concentration of bases and environmentally unfriendly organic solvents. Therefore, much attention has been paid to the development of heterogeneous catalytic systems that use clean and atom efficient oxidants like molecular oxygen or H_2O_2 without organic solvents.[55-66]

Recently, the aerobic oxidation of alcohols was successfully carried out by using heterogeneous catalysts such as tetrapropylammonium perruthenate (TPAP)/MCM-41,[59] Ru/CeO_2,[60] Ru-hydrotalcite,[61] Ru/hydroxyapatite (Ru-HAP),[62] $[RuCl_2(p\text{-cymene})]_2$/activated carbon,[63] Ru/Al_2O_3,[64] Pd-hydrotalcite which requires the addition of pyridine,[65] and Pd or Pt on activated carbon.[65, 66] These systems require the use of organic solvents. Wu et al. reported on solvent-free aerobic oxidation of alcohols by Pd/Al_2O_3.[67] However, the use of the noble metal, Pd is an essential requirement. Despite the advantage of using heterogeneous catalysts without organic solvents nor additives for oxidation of alcohols, few report has appeared on the use of highly active solvent-free heterogeneous catalysts with only molecular oxygen as oxidant.

In this respect, photoreactions are promising processes and the development of photocatalysts is a subject that is now receiving noticeable attention. TiO_2 has been identified as one example of a practical and useful photocatalysts,[68–71] and widely used in degradation of organic pollutants in air and water. However, in the most part of these reports, TiO_2 is used in vapor phase oxidations at high temperature,[67] oxidation of only lower

alcohols,[69, 70] oxidation using solvents such as benzene[71] and a low selectivity to partial oxidized products due to excess photo-activation of target products which leads to deep oxidation. Zhao et al[72, 73] reported that the photooxidation of alcohols on TiO_2 could be dramatically accelerated without any loss of selectivity by adsorption of Brønsted acid and this effect by Brønsted acid results from the decomposition of the relatively stable side-on peroxide promoted by the protons, which effectively clean the catalytic Ti-OH_2 sites. However, this system requires the use of benzotrifluoride as a solvent.

Recently, we found the photooxidation of alcohols to carbonyl compounds proceeded selectively at low temperature over Nb_2O_5 without organic solvents nor any additives (Table 3).[74-76] Various metal oxides (SiO_2, MgO, Al_2O_3, ZrO_2, V_2O_5, Ta_2O_5, MoO_3, and WO_3) showed no activity and the activity of ZnO was very low. TiO_2 showed higher activity than Nb_2O_5, however, the Nb_2O_5 catalyst showed higher selectivity than TiO_2 at the same conversion level.[74] Nb_2O_5 is suitable for selective oxidation. The photooxidation did not take place in the dark. Autooxidation proceeded when 1-phenylethanol, cyclohexanol and benzylalcohol were irradiated without catalyst. This was due to the formation of radical species by the photo-decomposition of carbonyl compounds (Norrish Type I reaction) which were present as impurities in the alcohols (entries 1 to 3). Nb_2O_5 catalyst improved the conversions and/or selectivities to carbonyl compounds greatly. The less reactive primary alcohol, 1-pentanol was also photooxidized over the Nb_2O_5 catalyst. The Nb_2O_5 catalyst was reusable and showed the same conversion and selectivity without any pretreatment as the catalyst as prepared.

3.2 Mechanism of photooxidation of alcohol over Nb_2O_5

The adsorbed species and intermediates of photooxidation were identified by *in situ* FT/IR spectra of adsorbed cyclohexanol on Nb_2O_5. Figure 8 shows the FT/IR spectra of adsorbed cyclohexanol on Nb_2O_5. The bands at 1467 and 1452 cm^{-1} were assigned to $\delta_s(CH_2)$ and the bands at 1363 and 1347 cm^{-1} were assigned to $\omega(CH_2)$, respectively. The new bands at 1091 and 1126 cm^{-1} appeared after the adsorption of cyclohexanol on Nb_2O_5. Therefore, these bands are assigned to the stretching mode of a C-O bond in the alcoholate species on the Nb_2O_5, because the formation of the alcoholate species by the adsorption of alcohol is usually accompanied by a shift of the stretching mode of a C-O bond to a higher wavenumber.[77-79] The change in FT/IR spectra by UV irradiation (< 390 nm) was shown in Fig. 9. The intensity of the band assigned to ν(C-O) (around 1090 cm^{-1}) decreased as the irradiation time increased, whereas the bands assigned to ν(C=O) (1676 cm^{-1}) and the symmetric-stretching of the carboxylic acid anion (1554 cm^{-1}) gradually grew. This result indicates that the alcoholate species on Nb_2O_5 was excited by photons and oxidized to carbonyl compounds. Interestingly, the carbonyl compounds were formed even under visible light irradiation (> 390 nm).

Figure 10 shows the EPR spectra of Nb_2O_5. A broad EPR signal around g = 1.9 was observed at 123 K (Fig. 9 (c)), when 1-pentanol was adsorbed on Nb_2O_5 under UV-irradiation. This broad signal at g = 1.9 was assignable to Nb^{4+} [80, 81] and immediately disappeared by the exposure to O_2 in the dark, indicating that Nb^{4+} was oxidized to Nb^{5+} rapidly even at 123 K. On the other hand, when 1-pentanol was adsorbed on Nb_2O_5 under UV-irradiation at 77K, EPR signal (g = 2.006, A_{H1} = 2.0 mT, A_{H2} = 4.4 mT) assigned to alkenyl radical species was observed (Fig. 11). These new signals were stable at 77 K without photo-irradiation, but disappeared at room temperature. The signal was restored by UV-irradiation at 77 K. Moreover, the signal did not change in the presence of O_2 even under UV-irradiation (Fig. 11 (f)).

Table 3 Photooxidation of various alcohols over Nb_2O_5 with molecular oxygen [a, b]

Entry	Substrate	Product	T / h	Conv. (%)	Sel. (%)
1	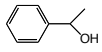	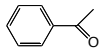	240 (72)	99 (14)	96 (69)
2	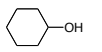	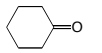	168 (96)	76 (46)	64 (36)
3	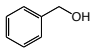	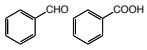	72 (72)	67 (79)	90 (43)
4	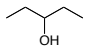		168 (119)	23 (2)	85 (82)
5	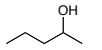		192 (121)	18 (5)	83 (81)
6	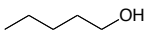	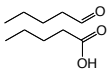	84 (24)	14 (0)	92 (-)

[a] Reaction conditions were as follows: alcohol (10 mL), Nb_2O_5 (100 mg), 323 K, under 0.1 MPa of O_2, O_2 flow rate (2 cm^3 min^{-1}): conversion and selectivity were determined by gas chromatography with an internal standard.

[b] Figures in parentheses are the results of photochemical reaction without catalysts.

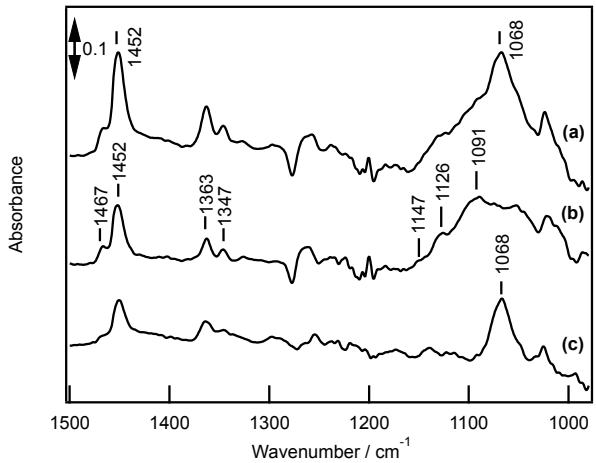

Fig. 8 FT-IR spectra of adsorbed cyclohexanol on Nb_2O_5. (a) cyclohexanol was exposed to Nb_2O_5 for 1 h (physisorption + chemisorption), (b) evacuated for 2 h (chemisorption), (c) difference spectrum ((a)-(b): physisorption) . Nb_2O_5 was evacuated at 773 K for 1 h and oxidized at 773 K with 10.7 kPa of O_2 and then evacuated at 773 K for 1 h before FT-IR measurements.

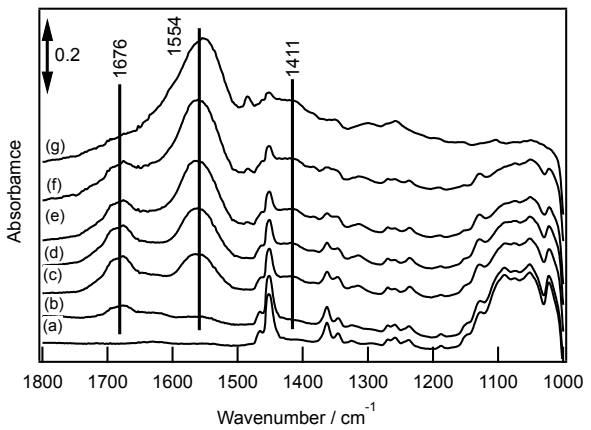

Fig. 9 FT-IR spectra of adsorbed species on Nb_2O_5 in the photo-reaction of adsorbed cyclohexanol with O_2. (a) cyclohexanol was exposed to Nb_2O_5 for 1 h and evacuated for 2 h, (b) under UV irradiation for 1, (c) 5 , (d) 7 , (e) 10 , (f) 15 and (g) 30 min. Nb_2O_5 was evacuated at 773 K for 1 h and oxidized at 773 K with 10.7 kPa of O_2 and then evacuated at 773 K for 1 h before FT-IR measurements.

This indicates that the alkenyl radical species dose not react with O_2. Therefore, it is suggests that 1) the photo-formed electron is trapped on Nb^{5+} to form Nb^{4+} and positive hole is captured by alcoholate species to convert to active alkenyl radical, 2) the active alkenyl radical is dehydrogenatied to carbonyl compound (the reduction of Nb^{5+} to Nb^{4+} takes place simultaneously), and 3) O_2 in the gas phase re-oxidizes Nb^{4+} to Nb^{5+}.

On the basis of these results, we proposed the reaction mechanism as shown in Scheme 3 [75-77]; 1) alcohol is adsorbed on Nb_2O_5 as alcoholate species, 2) alcoholate adsorbed on Nb_2O_5 is activated by transferring an electron to the conduction band reducing Nb^{5+} to Nb^{4+} and leaving a hole on alcoholate, 3) the formed alkenyl radical is converted to carbonyl compound, 4) the product desorbs, and 5) the reduced Nb^{4+} sites are re-oxidized by the reaction with O_2.

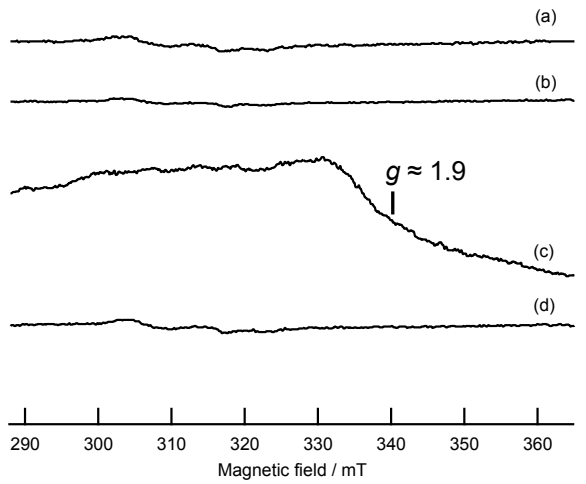

Fig. 10 ESR spectra of Nb_2O_5 recorded at 123 K. (a) after pretreatment, (b) in the dark in the presence of 1-pentanol, (c) under irradiation for 5 h in the presence of an excess of 1-pentanol, (d) after introduction of O_2. Nb_2O_5 was evacuated at 773 K for 1 h and oxidized at 773K with 10.7 kPa of O_2 and then evacuated at 773 K for 1 h before ESR measurements.

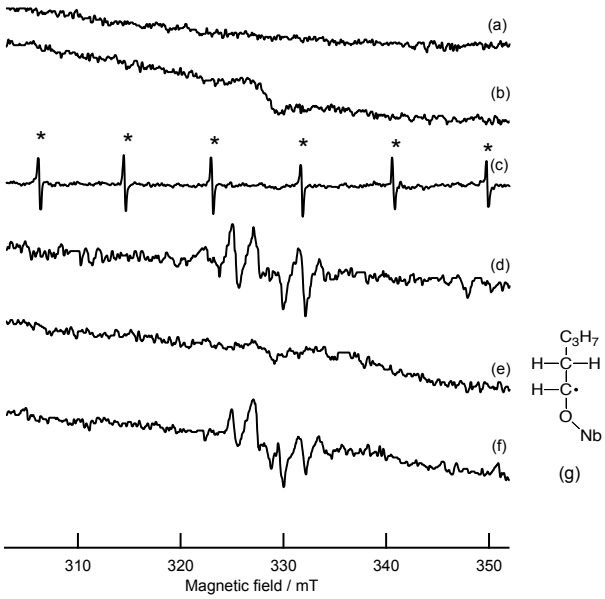

Fig. 11 ESR spectra of Nb_2O_5 recorded at 77 K. (a) after pretreatment, (b) under irradiation, (c) in the dark in the presence of 1-pentanol, (d) under irradiation in the presence of 1-pentanol, (e) in the dark after the sample was heated up to RT and then cooled to 77 K, (f) under re-irradiation. Nb_2O_5 was evacuated at 773 K for 1 h and oxidized at 773 K with 10.7 kPa of O_2 and then evacuated at 773 K for 1 h before ESR measurements. (g) alkenyl radical

In this mechanism, oxygen anion radical species (O_2^- and O_3^-), which are formed by irradiation over TiO_2[80-87] and often responsible for total oxidation, do not contribute to the photooxidation over Nb_2O_5. For instance, when Nb_2O_5 was irradiated in the presence of O_2, no EPR signal due to oxygen anion radical species was observed. This presumably explains why the photooxidation of alcohol to carbonyl compound proceeds selectively over the Nb_2O_5 catalyst.

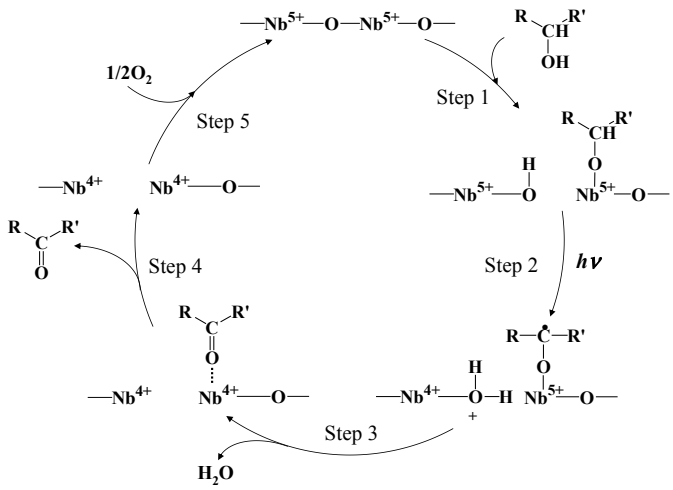

Scheme 3 Reaction mechanism of alcohol photooxidation with molecular oxygen over Nb_2O_5

We carried out the photooxidation of 1-pentanol under the various concentration of 1-pentanol, O_2 and the different light intensity to determine each reaction order. On the basis of these

results, the reaction rate (r) of photooxidation of alcohol is expressed as [Eq.(3)].

$$r = k\,[S]^{0.19}\,P_{O2}^{0.19}\,I^{0.65} \quad (3)$$

The rate constant, the substrate concentration, the light intensity and the pressure of the oxygen are abbreviated to k, [S], I and P_{O2}, respectively. By comparing the obtained rate equation [Eq. (3)] with the rate equation derived from the proposed reaction mechanism by steady-state approximation, it is suggested that Step 3 or Step 4 is the rate-determining step of the photooxidation of alcohol over Nb_2O_5. The alkenyl radical species was not obtained at 123 K, whereas Nb^{4+} was observed. This suggests that Step 3, the conversion of formed alkenyl radical to carbonyl compound took place even at 123 K because of a high reactivity of the alkenyl radical species. FT/IR spectra showed that the carbonyl compounds remained on the surface of Nb_2O_5 at room temperature, indicating that the desorption of the carbonyl compound was slow. Therefore, we concluded that the rate-determining step of the photooxidation of alcohol over Nb_2O_5 is Step 4, the desorption process of the formed carbonyl compound.

3.3 Mechanism of formation of alkenyl radical over Nb_2O_5

Figure 12 shows the apparent quantum efficiency of photooxidation of 1-pentanol as a function of the wavelength of the incident light (action spectrum) and a UV-Vis spectrum of Nb_2O_5. Although Nb_2O_5 catalyst is not able to absorb visible light (> 390 nm), the photooixdation of 1-pentanol took place under irradiation up to ca. 480 nm. This result is consistent with the change in the FT/IR spectra under visible light irradiation and a red shift of the effective wavelength of photo-reaction is similar to that of photo-SCR over TiO_2. In the case of photo-SCR over TiO_2, we found that the adsorbed NH_3 was photo-activated by the direct electron transfer from N 2p electron donor level formed between O 2p and Ti 3d of TiO_2 to the conduction band.[27]

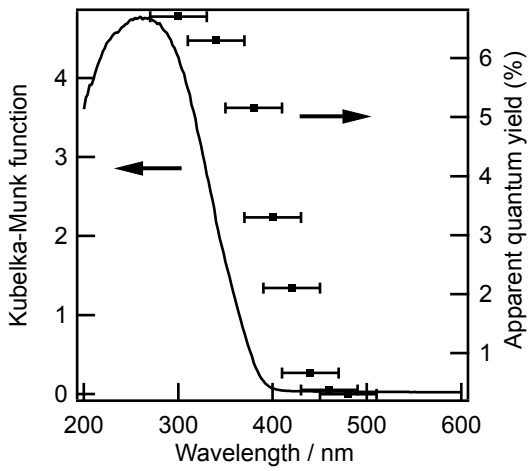

Fig. 12 Action spectrum of photooxidation of 1-penanol (dot) and UV-Vis spectrum of Nb_2O_5 (liner). Reaction conditions of the action spectrum were as follows: 1-pentanol (10 ml), Nb_2O_5 (100 mg), 323 K, under 0.1 MPa of O_2, O_2 flow rate (2 $cm^3\,min^{-1}$).

In order to investigate the formation of a new energy level derived form adsorbed molecule, DFT calculations were employed and showed that donor levels were generated between the HOMO and LUMO levels of Nb_2O_5 by adsorbed alcohol on Nb_2O_5 and that the electron transitions from O 2p donor level derived from the adsorbed alcoholate species to the conduction band of Nb_2O_5 (Nb 4d orbitals) had lower energy than those from O 2p of Nb_2O_5 (the conduction band) to Nb 4d.[75] On the basis of these results, we concluded that the photooxidation of alcohol over Nb_2O_5 takes place through the direct electron transfer from the O 2p orbital of adsorbed alcoholate species to the conduction band consisting of Nb 4d orbitals as shown in Fig. 13 ("*in situ doping*"). As a result of "*in situ doping*", the photooxidation of alcohol proceeded even under visible light irraidiation.

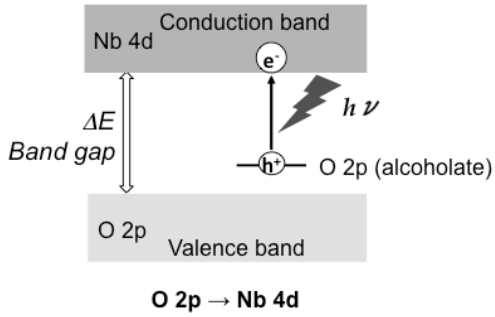

Fig. 13 Formation mechanism of alkenyl radical over Nb_2O_5

Conclusions and outlook

By means of UV-Vis, ESR, FT/IR with the aid of kinetic study and DFT calculations, the detailed reaction mechanisms of photo-assisted selective reduction of NO with NH_3 (photo-SCR) over TiO_2 and photooxidation of alcohol with O_2 over Nb_2O_5 were revealed and unique photo-activation mechanism by "*in situ doping*" in both photo-SCR and photooxidation of alcohol was demonstrated.

TiO_2 acts as an effective catalyst for photo-SCR even at room temperature. In this photo-SCR system, the re-heating of catalyst bed is unnecessary because of their possibility of application at low temperatures. Thus, photo-SCR system can miniaturize the reactor. Moreover, in this photo-SCR system, TiO_2 photocatalyst can activate NH_3 effectively even in the presence of excess O_2. Indeed, we found that TiO_2 acts as an effective catalyst for photo-assisted selective catalytic oxidation of NH_3 (photo-SCO: $4NH_3 + 3O_2 \rightarrow 2N_2 + 6H_2O$).[85-87] Although further improving the activity may be needed, it seems that this photo-SCO system can be used for removing unreacted NH_3 in the SCR process and for removing NH_3 from small and isolated source such as daily firm.

Photooxidation of alcohols to carbonyl compounds proceed selectively over Nb_2O_5 without organic solvents. Nb_2O_5 shows higher selectivity to partial oxidation product than that of commonly used TiO_2 photocatalyst, and efficient conversion under a solvent-free condition.

In the case of photo-SCR over TiO_2, a new electron donor (N 2p) was located between O 2p and Ti 3d by the adsorption of NH_3 on TiO_2. The direct electron transition from N 2p to Ti 3d took place to form NH_2 radical species by visible light irradiation. As a result, the photo-SCR proceeded even under visible light irradiation. The high activity of TiO_2 was caused by the expansion of the effective wavelength of TiO_2 by adsorption of NH_3 and the long lifetime of NH_2 radical. In the case of

photooxidation of alcohol over Nb_2O_5, as well as the adsorbed NH_3 on TiO_2, the new electron donor level was generated between O 2*p* and Ti 3*d* by the adsorption of alcohol on Nb_2O_5. The direct electron transition from O 2*p* derived from alcohol to Ti 3*d* took place to form alkenyl radical species by photo-irradiation. Then, this alkenyl radical was immediately dehydrogenated to carbonyl compound. As shown in the present review, the unique photo-activation mechanism by "*in situ doping*" gives us attractive ways for the removing the limit of bandgap energy, and the utilization of visible light.

Acknowledgements

A part of this work was partially supported by Grants-in-Aid for Scientific Research from the Ministry of Education, Culture, Sports, Science and Technology, Japan.

Notes and references

Department of Molecular Engineering, Graduate School of Engineering, Kyoto University, 1 Katsura, Nishikyo-ku, Kyoto 615-8510, Japan. Fax: +81 75-383-2561; Tel: +81 75-383-2559; E-mail: shishido@moleng.kyoto-u.ac.jp

† Electronic Supplementary Information (ESI) available: [details of any supplementary information available should be included here]. See DOI: 10.1039/b000000x/

‡ Footnotes should appear here. These might include comments relevant to but not central to the matter under discussion, limited experimental and spectral data, and crystallographic data.

1. S. Cho, *Chem. Eng. Prog.*, 1994, **90**, 39-45.
2. P. Forzatti, L. Lietti, *Heterogen. Chem. Rev.*, 1996, **3**, 33-51.
3. F. Nakajima, *Syokubai*, 1990, **32**, 236-239.
4. S. Wood, *Chem. Eng. Prog.*, 1994, **90**, 32-38.
5. A. Kato, S. Matsuda, F. Nakajima, M. Imanari, Y. Watanabe, *J. Phys. Chem.*, 1981, **85**, 1710-1713.
6. K. Otto, M. Shelef, J. T. Kummer, *J. Phys. Chem.*, 1970, **74**, 2690-2696.
7. F. Janssen, F. Van den Kerkhof, H. Bosch, J. J. Ross, *Phys. Chem.*, 1987, **91**, 5931-5934.
8. F. Janssen, F. Van den Kerkhof, H. Bosch, J. J. Ross, *Phys. Chem.*, 1987, **91**, 6633-6637.
9. B. Duffy, H. Curryhyde, N. Cant, *J. Phys. Chem.*, 1994, **98**, 7153-7161.
10. U. Ozkan, Y. Cai, M. W. Kumthekar, *J. Catal.*, 1994, **149**, 375-389.
11. U. Ozkan, Y. Cai, M. W. Kumthekar, *J. Phys. Chem.*, 1995, **99**, 2363-2371.
12. V. Parvulescu, P. Grange, B. Delmon, *Catal. Today*, 1998, **46**, 233-316.
13. R. Long, R. Yang, *J. Catal.*, 2002, **207**, 158-165.
14. L. Singoredjo, R. Korver, F. Kapteijn, J. Moulijn, *Appl. Catal. B*, 1992, **1**, 297-316.
15. M. Richter, A. Trunschke, U. Bentrup, K. Brzezinka, E. Schreier, M. Schneider, M. Pohl, R. Fricke, *J. Catal.*, 2002, **206**, 98-113.
16. E. Garcia-Bordeje, J. Pinilla, M. Lazaro, R. Moliner, J. Fierro, *J. Catal.*, 2005, **233**, 166-175.
17. G. Qi, R. Yang, *Chem. Commun.*, **2003**, 848-849.
18. D. Pena, B. Uphade, P. Smirniotis, *J. Catal.*, 2004, **221**, 421-431.
19. L. Gang, B. Anderson, J. van Grondelle, R. van Santen, *Catal. Today*, 2000, **61**, 179-185.
20. N. Cant, J. R. Cole, *J. Catal.*, 1992, **134**, 317-330.
21. T. Tanaka, K. Teramura, T. Funabiki, *Phys. Chem. Chem. Phys.*, 2000, **2**, 2681-2682.
22. T. Tanaka, K. Teramura, T. Yamamoto, S. Takenaka, S. Yoshida, T. Funabiki, *J. Photoch. Photobio. A*, 2002, **148**, 277-281.
23. T. Tanaka, K. Teramura, K. Arakaki, T. Funabiki, *Chem. Commun.*, **2002**, 2742-2743.
24. K. Teramura, T. Tanaka, T. Funabiki, *Langmuir*, 2003, **19**, 1209-1214.
25. K. Teramura, T. Tanaka, S. Yamazoe, K. Arakaki, T. Funabiki, *Appl. Catal. B*, 2004, **53**, 29-36.
26. K. Teramura, T. Tanaka, T. Funabiki, *Chem. Lett.*, 2003, **32**, 1184-1185.
27. S. Yamazoe, K. Teramura, Y. Hitomi, T. Shishido, T. Tanaka, *J. Phys. Chem. C*, 2007, **111**, 14189-14197.
28. S. Yamazoe, T. Okumura, K. Teramura, T. Tanaka, *Catal. Today*, 2006, **111**, 266-270.
29. S. Yamazoe, Y. Masutani, Y. Hitomi, T. Shishido, T. Tanaka, *Appl. Catal. B*, 2008, **83**, 123-130.
30. P. Meriaudreau, M. Che, C. K. Jorgensen, *Chem. Phys. Lett.*, 1970, **5**, 226-228.
31. C. Hauser, P. Naccache, *Chem.Phys. Lett.*, 1971, **8**, 45-48.
32. R. F. Howe, M. Gratzel, *J. Phys. Chem.*, 1985, **89**, 4495-4499.
33. D. Hurum, A. G. Agrios, K. A. Gray, T. Rajh, M. C. Thurnauer, *J. Phys. Chem. B*, 2003, **107**, 4545-4549.
34. S. N. Forer, E. L. Cochran, V. A. Bowers, C. K. Jen, *Phys. Rev. Lett.*, 1958, **1**, 91-94.
35. E. F. Vansant, J. H. Lunsford, *J. Phys. Chem.*, 1972, **76**, 2716-2718.
36. O. I. Brotikovskii, G. M. Zhidomirov, V. B. Kazanskii, A. I. Mashchenko, B. N. Shelmimov, *Kinet. Katal.*, 1971, **12**, 616-619.
37. S. Nagai, *Bull. Chem. Soc. Jpn.*, 1973, **46**, 1144-1148.
38. N. Shimamoto, K. Hatano, T. Katsu, Y. Fujita, *Bull. Chem.Soc. Jpn.*, 1975, **48**, 18-21.
39. G. Ramis, G. Busca, F. Bregani, P. Forzatti, *Appl. Catal.*, 1990, **64**, 259-278.
40. M. C. Kung, H. H. Kung, *Catal. Rev.-Soc. Eng.*, 1985, **27**, 425-460.
41. C. C. Chuang, J. S. Shiu, L. J. Lin, *Phys. Chem. Chem. Phys.*, 2000, **2**, 2629-2633.
42. E. Ito, Y. J. Mergler, B. E. Nieuwenhuys, H. P. A. Calis, H. vanBekkum, C. M. vandenBleck, *J. Chem. Soc., Faraday Trans.*, 1996, **92**, 1799-1806.
43. H. Einga, S. Futamura, T. Ibusuki, *J. Jpn. Pttrol. Int.*, 1999, **42**, 363-364.
44. H. Einga, S. Futamura, T. Ibusuki, *Phys. Chem. Chem. Phys.*, 1999, **1**, 4903-4908.
45. H. Einga, S. Futamura, T. Ibusuki, *Appl. Catal. B.-Environ.*, 2002, **38**, 215-225.
46. S. Ikeda, N. Sugiyama, B. Pal, G. Macri, L. Palmisano, H. Noguchi, K. Uosaki, B. Ohtani, *Phys. Chem. Chem. Phys.*, 2001, **3**, 267-273.
47. S. Ikeda, N. Sugiyama, S. Murakai, H. Kominami, Y. Kera, H. Noguchi, K. Uosaki, K. Torimoto, B. Ohtani, *Phys. Chem. Chem. Phys.*, 2003, **5**, 778-783.
48. R. Asahi, T. Morikawa, T. Ohwaki, K. Aoki, Y. Taga, *Science*, 2001, **293**, 269-271.
49. S. Sato, *Chem. Phys. Lett.*, 1986, **123**, 126-128.
50. H. Luo, T. Takata, Y. Lee, J. Zhao, K. Domen, Y. Yan, *Chem. Mater.*, 2004, **16**, 846-849.
51. M. Miyauchi, A. Nakajima, T. Watanabe, K. Hashimoto, *Chem. Mater.*, 2002, **14**, 4714-4720.
52. R. A. Sheldon, J. K. Kochi, *Metal-Catalyzed Oxidations of Organic Compounds*, Academic Press, New York, 1981.
53. M. Hudlicky, *Oxidations in Organic Chemistry*, ACS Monograph Series, American Chemical Society, Washington, DC, 1990.
54. C. L.Hill, *Advances in Oxygenated Process, Vol. 1* (Eds.: A. L. Baumstark), JAI, London, 1998, p.1.
55. R. C. Larock, *Comprehensive Organic Transformations*, VCH, New York, 1989.
56. R. A. Sheldon, I. W. C. E. Arends, A. Dijksman, *Catal. Today*, 2000, **57**, 157.
57. T. Mallat, A. Baiker, *Chem. Rev.*, 2004, **104**, 3037-3058.
58. N. Srinivas, V. R. Rani, M. R. Kishan, S. J. Kulkarni, K. V. Raghavan, *J. Mol. Catal. A: Chem.*, 2001, **172**, 187-191.
59. A. Bleloch, B. F. G. Johnson, S. V. Ley, A. Price, D. S. Shephard, A. W. Thomas, *Chem. Commun.*, **1999**, 1907-1908.
60. F. Vocanson, Y. P. Guo, J. L. Namy, H. B. Kagan, *Synth. Commun.*, 1998, **398**, 1907-1908.
61. T. Matsushita, K. Ebitani, K. Kaneda, *Chem. Commun.*, **1999**, 265-266.
62. a) K. Yamaguchi, K. Mori, T. Mizugaki, K. Ebitani, K. Kaneda, *J. Am. Chem. Soc.*, 2000, **122**, 7144-7145. b) K. Mori, S. Kanai, T.

Hara, T. Mizugaki, K. Ebatani, K. Jitsukawa, K. Kaneda, *Chem. Mater.*, 2007, **19**, 1249-1256.
63. E. Choi, C. Lee, Y. Na, S. Chang, *Org. Lett.,* 2002, **4**, 2369-2371.
64. K. Yamaguchi, N. Mizuno, *Angew. Chem. Int. Ed.*, 2002, **41**, 4538-4540.
65. N. Kakiuchi, Y. Maeda, T. Nishimura, S. Uemura, *J. Org. Chem.,* 2001, **66**, 6620-.6623
66. T. Mallat, A. Baiker, *Catal. Today,* 1994, **19**, 247-283.
67. H. Wu, Q. Zhang, Y. Wang, *Adv. Synth. Catal.*, 2005, 347, 1356-1357.
68. U. R. Pillai, E. S. Demessie, *J. Catal.*, 2002, 211, 434-444.
69. J. Chen, D. F. Ollis, W. H. Rulkens, H. Bruning, *Water Res.*, 1999, **33**, 661-668.
70. a) D. S. Muggli, J. T. Mccue, J. L. Falconer, *J. Catal.*, 1998, **173**, 470-483. b) J. L. Falconer, K. A. M. Bair, *J. Catal.*, 1998, **179**, 171-178.
71. F. H. Hussein, G. Pattenden, R. Rudham, J. J. Russell, *Tetrahedron Lett.*, 1984, **25**, 3363-3364.
72. M. Zhang, Q. Wang, C. Chen, L. Zang, W. Ma, J. Zhao, *Angew. Chem. Int. Ed.*, 2009, **48**, 6081-6084.
73. Q. Wang, M. Zhang, C. Chen, W. Ma, J. Zhao, *Angew. Chem. Int. Ed.*, 2010, **49**, 7976-7979.
74. T. Ohuchi, T. Miyatake, Y. Hitomi, T. Tanaka, *Catal. Today*, 2007, **120**, 233-239.
75. T. Shishido, T. Miyatake, K. Teramura, Y. Hitomi, T. Tanaka, *J. Phys. Chem. C*, 2009, **113**, 18713-18718.
76. S. Furukawa, Y. Ohno, T. Shishido, K. Teramrau, T. Tanaka, *Syokubai*, 2011, **53**, 132-134.
77. L. H. Little, A. V. Kiselev, V. I. Lygin, *Infrared Spectra of Adsorbed Species*, Academic Press Inc., London, **1966**.
78. G. Socrates, *Infrared Characteristic Group Frequencies: Table and Charts*, Wiely, New York, **1994**.
79. V. Z. Fridman, A. A. Davydov, K. Titievsky, *J. Catal.*, 2004, **222**, 545-557.
80. M. Sugantha, U. V. Varadaraju, *J. Solid State Chem.*, 1994, **111**, 33-40.
81. C. Veríssimo, F. M. S. Garriodo, O. L. Alves, P. Calle, A. Martínez-Juárez, J. E. Iglesias, J. M. Rojo *Solid State Ionics*, 1997, **100**, 127-134.
82. P. Meriaudeau, J. C. Vedrine, *J. Chem. Soc. Faraday I*, 1976, **72**, 472-480.
83. A. R. Gonzalez-Elipe, G. Munuera, J. Soria, *J. Chem. Soc. Faraday I*, 1979, **75**, 748-761.
84. Y. Nakaoka, Y. Nosaka, *J. Photochem. Photobiol. A*, 1997, **110**, 299-305.
85. S. Yamazoe, T. Okumura, T. Tanaka, *Catal. Today*, 2007, **120**, 220-225.
86. S. Yamazoe, T. Okumura, Y. Hitomi, T. Shishido, T. Tanaka, *J. Phys. Chem. C*, 2007, **111**, 11077-11085.
87. S. Yamazoe, Y. Hitomi, T. Shishido, T. Tanaka, *Appl. Catal. B*, 2008, **82**, 67-76.